ADVANCED FUNCTIONAL MATERIALS
www.afm-journal.de

A Rubberlike Stretchable Fibrous Membrane with Anti-Wettability and Gas Breathability

*Seong J. Cho, Hyoryung Nam, Hyobong Ryu, and Geunbae Lim**

The fabrication of a stable, anti-wetting surface is a very challenging issue in surface chemistry. In general, superhydrophobicity highly depends on the surface structure. Moreover, mechanical deformation of the surface structure can produce dramatic changes in the surface wetting state, and in some cases, may even result in a complete loss of the surface's unique wettability. However, the study of stable surfaces under mechanical deformation conditions has been limited to flexible surfaces or small strain. Here, a mechanically stable superhydrophobic membrane is presented, which possesses high stretchability and gas breathability. The membrane, which consists of an elastic polyurethane fibrous matrix coated with polyaniline hairy nanostructures and polytetrafluoroethylene, exhibites excellent superhydrophobic properties under ≥300% strain. The breathability and wettability of the membrane is examined by examining various static and dynamic wetting parameters. The robust membrane maintaines its anti-wettability (water contact angle ≈160°, hysteresis ≈10°) for 1000 stretching cycles. It is also determined that the stretchable and superhydrophobic surface suppresses the fragmentation and rebound of impact droplets, compared with rigid superhydrophobic surfaces. Finally, underwater gas sensing is demonstrated as a novel application.

1. Introduction

A stable superhydrophobic surface is essential for realizing various functional applications such as self-cleaning,[1] anti-icing,[2] low-drag surfaces,[3] water harvest,[4] and liquid separation.[5] There have been a variety of reports on stable anti-wetting surfaces.[6–9] Lim et al. reported thermally stable superhydrophobic fabrics made using electrospinning and methyltriethoxysilane.[6] Fabrics that remain superhydrophobic after heat treatment at 500 °C were utilized for oil–water separation and as high-performance automobile air filters.[6] Tuteja et al. reported a superoleophobic surface that forms a high contact angle with organic liquids with surface tensions much lower than that of water. A liquid-independent anti-wetting surface was achieved by fabricating re-entrant structures using electrospinning and micromachining.[9] Recently, Deng et al. reported a mechanically stable anti-wetting surface on glass using candle soot as a template.[10] The surface not only exhibited anti-wettability, but also proved to be extremely durable in its resistance to sand abrasion. However, studies of mechanically stable surfaces under dynamic conditions, such as mechanical deformation of the substrate, have been limited to flexible surfaces or small strain.[11–15] In general, significant mechanical deformation damages the surface, possibly changing its micro/nanostructure; this structure plays a crucial role in the superhydrophobicity of the surface.[16–18] Wu et al. reported that the wetting state can be changed by just curving a deformable substrate.[18] However, for deformable anti-wetting applications a mechanically stable superhydrophobic surface is necessary. For instance, a gas-breathable, waterproof fabric such as expanded polytetrafluoroethylene (e-PTFE) has a very low yield strain of ca. 10%.[19] If e-PTFE were stretchable, the fabrics would be more comfortable and more resistant to deformation during machine washing. Recently, stretchable electronics have received great interest, and various electronic material devices have been reported. To our knowledge, however, there is no report on an anti-wetting surface for packaging highly stretchable devices. Consequently, the challenge has been to find surfaces that maintain their wettability under dynamic deformation conditions.

Here, we report on the performance of a novel, durable, superhydrophobic fibrous membrane under extremely harsh deformation conditions. This membrane showed excellent superhydrophobic properties under ≥300% strain, maintaining its wetting behavior for 1000 stretching cycles. During the high deformation application, nanocracks formed in the microfibers. To better understand this effect, we analyzed the morphological change and the wetting behavior of the cracks. Droplet impact on solid surfaces is a key phenomenon encountered in practical applications, such as ink-jet printing, spray coating, water cleaning or cooling, and the combustion of liquid fuels.[20]

S. J. Cho, H. Ryu
Department of Mechanical Engineering
Pohang University of Science and Technology (POSTECH)
Pohang, Gyungbuk, 790-784, Republic of Korea
H. Nam
Division of Integrative Bioscience and Biotechnology
Pohang University of Science and Technology (POSTECH)
Pohang, Gyungbuk, 790-784, Republic of Korea
Prof. G. Lim
Department of Mechanical Engineering
Division of Integrative Bioscience and Biotechnology
Pohang University of Science and Technology (POSTECH)
Pohang, Gyungbuk, 790-784, Republic of Korea
E-mail: limmems@postech.ac.kr

DOI: 10.1002/adfm.201300442

Thus, along with the analysis of the membrane's static wetting properties, we also investigated the behavior of impact droplets on the membrane for various states of the substrate under dynamic conditions, using a high-speed camera. This is the first droplet impact study on a stretchable, superhydrophobic surface, which has not to our knowledge been described previously. Our results showed that the stretchable membrane suppressed fragmentation (e.g., splashing) and bouncing of the impact droplet, compared with rigid, superhydrophobic surfaces. Unlike typical superhydrophobic membranes, the electrospun matrix has numerous micropores in the membrane. These pores allow the penetration of gas, acoustic waves, and tiny particles; however, water is not allowed to pass. To verify the breathability, we evaluated the gas breathability using phenolphthalein (a pH indicator), ammonia solution, O_2 gas, and a sensor. Finally, we have demonstrated underwater gas sensing as a novel application.

Our functional membrane was fabricated based on simple and economical processes, and did not require high-vacuum equipment, accurate optics, or high thermal processes. The backbone of the stretchable membrane was fabricated by electrospinning, which is an easy and versatile method that is used to fabricate continuous ultrafine fibers.[21] of polyurethane (PU), one of the most elastic polymers. Stable superhydrophobicity can be achieved using nanostructures on the order of 100 nm or less, as shown in the Lotus leaf in nature.[22] As such, for this study, the PU fibers were coated with polyaniline (PANI) hairy nanostructures using a dilute polymerization technique developed recently.[23] Dilute polymerization is a simple, low-temperature, self-assembly method, which can be used to coat numerous surfaces, regardless of material or morphology.[23] Finally, the superhydrophobic fibrous membrane with enhanced stretchability was obtained after dip-coating the membrane in polytetrafluoroethylene (PTFE), to achieve a low surface energy. The resulting stretchable, functional membrane should prove to be useful for many applications, including functional fabrics, gas-sensor packaging, gas separators, and waterproof applications of stretchable electronics.

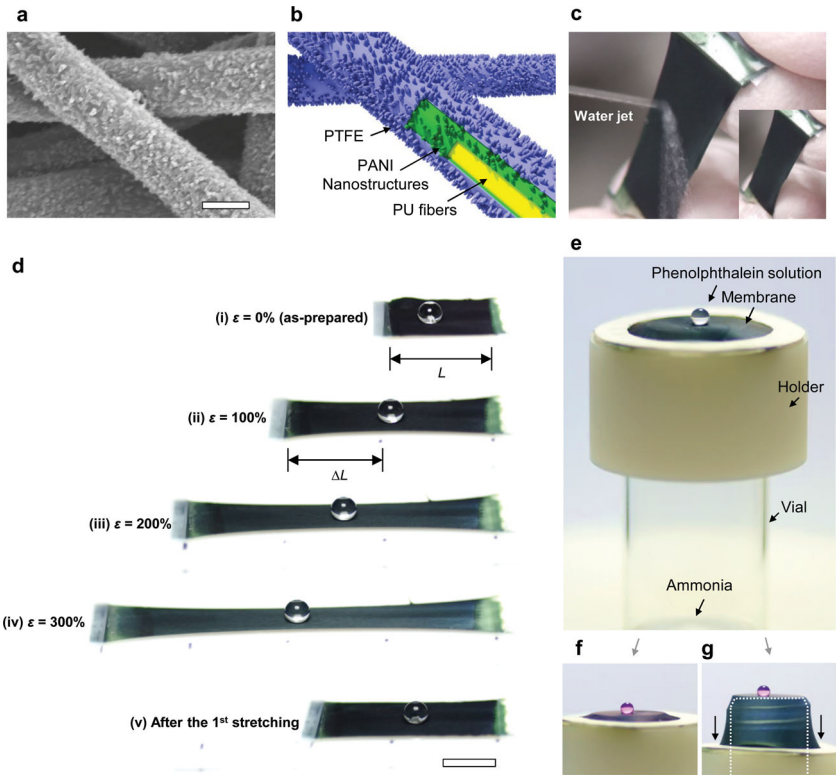

Figure 1. Highly stretchable, anti-wettable, and air-breathable nanostructured fibrous membrane. a) High-resolution scanning electron microscopy (HR-SEM) image of a polyaniline (PANI)-nanostructured polyurethane (PU) fibrous membrane. Scale bar: 1 µm. b) Schematic diagram of the membrane consisting of PU fibers, PANI nanostructures (≈40-nm diameter), and a polytetrafluoroethylene (PTFE) layer. c) Photograph showing the resistance to a water jet. After jetting, there were no remaining droplets (Inset: after jetting). d) Optical images of the superhydrophobic membrane under various strain, $\varepsilon = \Delta L/L \cdot 100$, ranging from 0 to 300%. The length of the membrane was restored to 1.5 times as long as the as-prepared length (v). The 10-µL droplets maintained their spherical shapes due to the anti-wettability of the membrane. Scale bar: 1 cm. e) Gas-breathability test using a phenolphthalein pH indicator solution and ammonia as a volatile base solution. f) The phenolphthalein droplet became reddish due to its reaction with ammonia gas, which passed through the porous membrane within a couple of seconds. g) The membrane can conform to a cylindrical geometry (white dotted line) while maintaining its anti-wettability and gas breathability.

2. Results and Discussion

Figure 1a,b shows a scanning electron microscope (SEM) image and a schematic diagram of the anti-wettable, stretchable, air-breathable nanostructured fibrous membrane, respectively. Uniform PU fibers, with a diameter of ca. 1 µm, were used to form the elastic backbone structure, which was produced by an electrospinning process. The PU microfibers were then coated with PANI hairy nanostructures (diameter: 20–40 nm; length: ≈100 nm), using a dilute PANI polymerization method,[23] as shown in Figure 1(a). This high-aspect ratio geometry minimizes the contact area with the liquid, which is a necessary condition for fabricating anti-wetting surfaces. The membrane was then coated with PTFE, one of the lowest surface energy materials available, to produce a highly stretchable, superhydrophobic membrane (the detailed experimental process is provided in the Experimental Section). The PTFE cover conformed to the PANI-nanostructured fibers (Figure S1 in the Supporting Information). The fiber diameter did not significantly affect the wettability because the nanostructures conferred the superhydrophobic property.[23] However, some thin fibers (diameter <200 nm) were hydrophobic, not superhydrophobic (Supporting Information Figure S2). The membrane exhibited excellent anti-wetting properties, demonstrating the ability to block falling droplets or even water jets. After continuous jetting,

there was no evidence of water residue. This was attributed to the water contact being in the form of a Cassie state, in which the liquid droplet resides on a composite surface composed of the solid and trapped air (see Figure 1c and the movie in the Supporting Information). According to the results of a uniaxial tensile test performed by a universal testing machine (UTM), our PU-based membrane demonstrated rubber-like hyperelastic properties over the entire strain range (Supporting Information Figure S3). The nanostructured membrane had a high maximum strain break point ($\varepsilon_{max} = \Delta L_{max}/L \cdot 100 =$ 350%), as well as a low modulus (≈1.4 MPa). Interestingly, the membrane maintained its superhydrophobic property over the entire strain range tested, up to the breaking point, as shown in Figure 1d. The wetting analysis will be presented in more detail in a later section. If the elongation stopped before the breaking of the fibers, and the applied force was removed, then the membrane tended to revert back to its original shape. After the first stretching cycle ($\varepsilon = 0\% \rightarrow 300\% \rightarrow 0\%$), the length of the membrane was restored to 1.5 times as long as the as-prepared length. (Picture (v) in Figure 1d); after the second and further stretching cycles, the length was restored to that after the first stretching cycle. This unrecoverable behavior exhibited by the membrane after the first stretching cycle was attributed to the slippage of crossed fibers and the breakage of the fibers at junctions.[24] Another possible cause could be the fracturing of the PANI structure (**Figure 2**) in the early strain regime ($\varepsilon \leq 40\%$; Supporting Information Figure S3) due to a mismatch between the PANI and PU moduli (PANI modulus ≈1 GPa,[25] PU modulus ≈1.2 MPa from our experimental results).

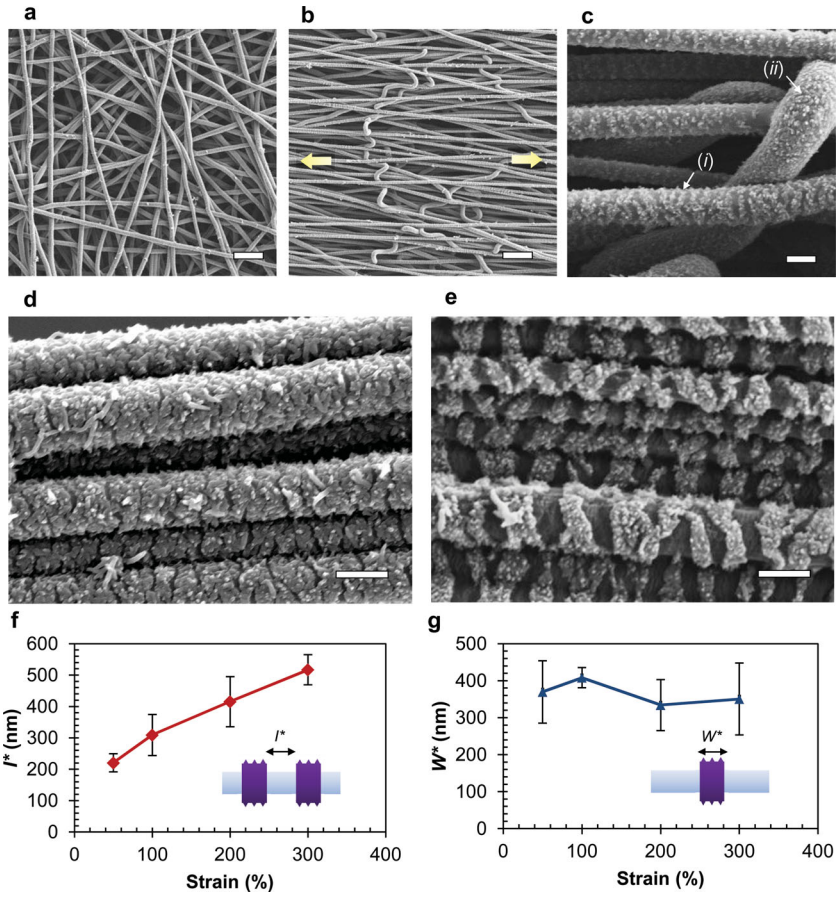

Figure 2. a) SEM image of randomly oriented nanostructured PU fibers (as-prepared). Scale bar: 10 µm. b) PU fibers shown in (a), horizontally stretched by 200% (in the direction of the yellow arrows). The stretched fibers were aligned in the stretched direction. Scale bar: 10 µm. c) Magnified image of (b). The PANI structures on the stretched fibers were slightly cracked (i); however, the fibers oriented orthogonal with respect to the stretch direction were not cracked (ii). Scale bar: 1 µm. d) 0% stretched fibers oriented in one direction, produced by a parallel collector. Scale bar: 1 µm. (e) 100% stretched image of (d). Scale bar: 1 µm. f,g) Interval spacing and crack width, *l** and *W**, respectively, as a function of strain.

The stretchable and superhydrophobic membrane had a microporous structure (>5-µm micropores), due to the stacking of randomly oriented microfibers, as shown in Figure 1a and Figure 2a. Therefore, the membrane demonstrated a selective breathability, i.e., it allowed gas flow, small droplets (e.g., moisture), and acoustic waves to pass through the pores; however, the membrane blocked water infiltration in aqueous environments. To verify the gas breathability of the membrane, a phenolphthalein pH indicator solution and an ammonia solution were used; the phenolphthalein solution turns a pink color when reacting to a strong base. The ammonia solution was used as a volatile base. Figure 1e shows the experimental setup for the gas-breathability experiment. A 5-mL ammonia solution was placed in a vial. The membrane was attached to a cylindrical plastic holder to maintain its shape as it came into contact with the ammonia vial. The phenolphthalein indicator solution was dropped onto the membrane, as shown in Figure 1e. The indicator droplet turned reddish in color upon dropping; the droplet color deepened over time as ammonia gas passed through the membrane and reacted with the solution (see Figure 1f and the movie in Supporting Information). We found that the membrane was easily deformable and could conform to a three-dimensional structure, such as a cylindrical vial, while maintaining its gas breathability (white dotted line in Figure 1g). This deformability of the membrane could be utilized in packaging applications requiring stretchable or complex-shaped devices.

2.1. Nanocracked Fibers

Due to the Young's modulus mismatch and high strain conditions, the generation of stress at the interface of the PANI-PU structure caused the surface to deform or fracture. We observed this change in the surface morphology using high-resolution SEM (HR-SEM), as shown in Figure 2a–e. The electrospun PU fibers were deposited onto a conductive collector as a randomly oriented mat, due to their chaotic whipping nature

(Figure 2a).[26] As mentioned earlier, the pores between the randomly oriented fibers play a crucial role in gas breathability. The average pore size was ca. 10 μm. As the membrane was stretched uniaxially (in the direction of the yellow arrows in Figure 2b), the randomly oriented fibers became aligned with the stretched direction. The alignment of the fibers improved as the strain on the fibers increased. In the PANI-nanostructured layer, the highly elongated fibers became slightly cracked, as shown in (i) of Figure 2c. However, the fibers that were oriented orthogonal with respect to the stretch direction did not crack, as shown in (ii) of Figure 2c. In other words, the angle between the fiber orientation and the stretching direction critically affected the formation of surface layer cracks. Additionally, the collected fibers had a coiling or wavy morphology. These non-straight morphologies created a difference between the apparent strain (the strain of the membrane, which we applied and measured) and the individual strain (the strain of a fiber). Cracks in the nanostructure can affect the wetting behavior and mechanical properties, such as durability. The ability to control and minimize crack formation in micro/nanofabrications has become a critical issue.[27] Thus, to analyze precisely the crack formation, we prepared one-directional oriented fibrous samples to prevent the unexpected effects. The one-directional fibers were fabricated using a patterned collector, discussed in our previous works.[28,29] Figure 2d,e shows 0 and 100% stretched fibers, respectively. The PANI structure cracked repeatedly orthogonal to the stretching direction along the entire fiber length, regardless of the membrane strain (Supporting Information Figure S4). The morphology of the cracked PANI structure was affected by the strain. In particular, the interval spacing between adjacent cracks increased with increasing strain, as shown in the graph of Figure 2f. The average interval distance was ca. 520 nm at a strain of 300%, and the maximum interval distance at the breaking point (ε_{max} = 350%) was estimated to be 550 nm, according to the data shown in Figure 2f. The width of the cracks at various strain values remained in the range of 300 to 400 nm.

The microscale fibers, the sub-microscale cracks, and the nanoscale PANI nanostructures produced a multi-scale hierarchical structure; this structure was essential to the stability of the superhydrophobic surface.[8] Hence, the structure could maintain stable anti-wettability. To verify that the sub-microscale gap was small enough to sustain anti-wetting, we calculated the maximum pressure (Δp_{max}) that the interface between the water and the crack gap could maintain in a Cassie state, using a simple geometric model and the Laplace equation (see details in the caption of Supporting Information Figure S5). In general, a superhydrophobic, self-cleaning surface is achieved by the formation of a composite interface, such as a solid–air interface like the one used for the Cassie state. According to our model, Δp_{max} can be calculated theoretically as follows:

$$\Delta p_{max} = \frac{8\gamma T^*}{I^{*2} + 4T^{*2}} \quad (1)$$

where I^*, T^*, and γ are the average interval, the thickness of the cracked structure, and the surface tension, respectively. For a nanostructured membrane undergoing 300% strain (Figure 2f), with I^* = 520 nm, T^* = 100 nm, and the surface tension, γ = 72 mN m^{-1} (water, 25 °C), Δp_{max} is 186 kPa. This pressure is sufficient for blocking high-speed droplets, such as falling raindrops. (The terminal velocity of a typical raindrop is around 10 m s^{-1}, corresponding to a dynamic pressure of 50 kPa.[30]).

2.2. Evaluation of Wettability

To evaluate the wettability of the membrane, a static contact angle (CA) and contact angle hysteresis (CAH) at various strains and stretching cycles were investigated using the sessile droplet method (**Figure 3**a,b). CA and CAH are basic indices used to

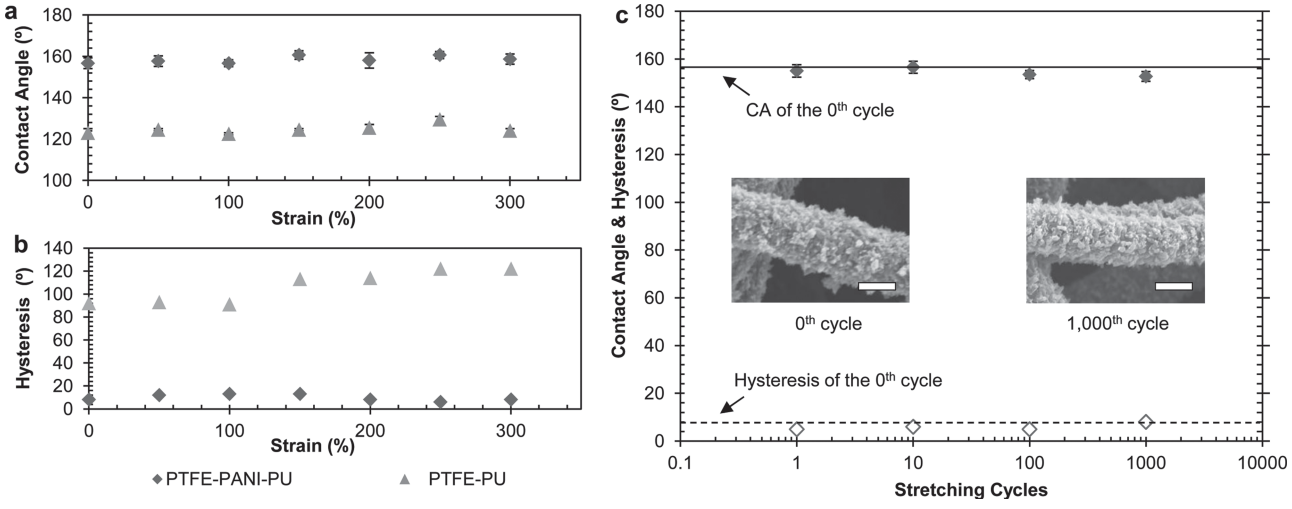

Figure 3. a) Static contact angle (CA) and b) CA hysteresis (CAH) of a PTFE-PU fibrous membrane (yellow triangles) and a PTFE-PANI-coated PU fibrous membrane (red diamonds) under various strains. The PANI-nanostructured surface maintained its superhydrophobicity at high CA (>150°) and low hysteresis (<10°), despite the high deformation of the membrane (strain of ≈300%). c) CAs (filled red diamonds) and CAHs (open red diamonds) of the stretchable membrane after a stretching cycle (strain of 100% → 300% → 100%). The insets are SEM images of a 0-cycle stretched fiber and a 1000-cycle stretched fiber. Scale bar: 1 μm. The membrane maintained its superhydrophobicity and fiber nanostructure after 1000 cycles.

characterize wettability. In general, superhydrophobic surfaces require a very high CA (>150°). Figure 3a represents the CAs of a PTFE-PU fibrous membrane and PTFE-PANI-coated PU fibrous membrane over the strain range of 0 to 300%. All of the PTFE-PU membranes had a similar CA of ≈125°, regardless of the strain. However, the average CA of the PANI-nanostructured PU membranes was 160.0°, due to the surface roughness. The CAH dramatically decreased from 106.7 to 9.7° for the PANI-nanostructured PU membranes (Figure 3b). The low CAH implies that the water–solid contact resided in the Cassie state, but not the Wenzel state. This was attributed to the low adhesive force of the solid–air composite interface in the Cassie state.[31] A high CA and low CAH are essential wetting properties for achieving unique functionalities of surfaces, such as self-cleaning and low-drag reduction.

Practical application of our stretchable membrane required the evaluation of its wettability while undergoing repetitive mechanical deformation. A cyclical stretching experiment was conducted for this evaluation. A cycle consisted of applying a low strain (100%) and then a high strain (300%), followed by the low strain (100%) once again. After repeated cycles, the CA and CAH were measured by a method used in previous works. Figure 3c shows the results of wetting behavior after cyclical stretching. The measured points were the 1st, 10th, 100th, and 1000th cycle. Up to the one 1000th cycle, the CA and CAH for our membrane sustained an average of 156° and 8°, respectively, almost as high as those of the as-prepared membrane (0th cycle). Although not indicated on the graph, the membrane maintained its anti-wettability with further cyclical stretching. Despite numerous cyclical deformations, the morphology of the surface did not appear to have changed, as shown in the insets of Figure 3c. The stability of the membrane structure is related to crack formation. The regularly formed cracks in the nanostructures of the fibers helped to release the interfacial stress that occurred during high deformation due to the modulus mismatch. Thus, the PANI nanostructure and PU fibers were combined robustly, and the fibrous architecture demonstrated stable anti-wettability against high deformation.

2.3. Dynamics of Droplet Impact

We also investigated how the stretchability affected the dynamics of droplet impact and how the effect on stretchable superhydrophobic surfaces differed from that of a rigid surface. Before analysis, we introduced two dimensionless factors: the Weber number (*We*) and the maximum spreading factor (D^*), which were related to the impact dynamics of the droplet. The *We* is the ratio of the kinetic energy to the surface energy, $\rho R_0 V^2_i/\gamma$, where ρ, R_0, V_i, and γ represent the density, the radius of the droplet before impact, the impact velocity, and the surface tension, respectively. D^*, calculated as R_{max}/R_0 with R_{max} corresponding to the maximum radius of the spreading droplet, indicates the surface tension energy transferred from the kinetic energy of the impact droplet.[32] **Figure 4**a shows sequential images of a droplet (V_i: 1.67 m s^{-1}; *We*: 53) impinging on the stretchable membrane with a strain of 100% and a rigid surface. The rigid surface was prepared using the same surface used for the stretchable membrane; however, the membrane was supported by a rigid aluminum block. A variety of phenomena were observed during the impact. In the case of the stretchable membrane, at the moment of impact, the membrane deflected downward with maximum deflection occurring at ≈1.7 ms. Simultaneously, a lamella emerged from under the droplet and spread further, reaching its maximum radius (R_{max}) at ≈4.7 ms. After spreading, the spread droplet bounced and returned to its former spherical shape. Finally, the bouncing droplet reached a maximum height (H_{max}). In the case of a rigid membrane, there was no deflection, and the lamella structure had a wavy perimeter and splashed under high *We* conditions (>44).

The droplet behavior was affected by the initial conditions, such as the substrate and *We*. Figure 4b shows that D^* increased with increasing *We*. This result is similar to the impact results of a droplet on a rigid, superhydrophobic surface, reported previously.[32,33] Additionally, we found that D^* was a function of strain in the case of a stretchable surface. According to our experiment, as the strain on the membrane decreased, D^* decreased at the same *We* (Figure 4b). In terms of energy, the low-strain membrane reduced the surface tension energy of the droplet transferred from its kinetic energy; the kinetic energy of the droplet was transformed into the elastic energy of the stretchable membrane.

Due to the variable energy distribution of the stretchable substrate, we observed differences in the splashing threshold velocity, morphology of the reflected droplets, and coefficient of restitution of the impact droplet. First, we observed that the occurrence of the splash was highly affected by the strain on the membrane; splashing could be suppressed by reducing the strain. This tendency agreed well with the results of droplet impact on a typical elastic membrane.[34] The thickness of the lamella at impact was inversely related to D^*, because the volume of the droplet was constant. The thickness was highly relevant to the occurrence of a splash, because a thin lamella increased the instability close to the rim.[20] Figure 4c reveals the threshold *We* at which splashing occurred as a function of strain; the Figure is divided into the splash regime (*I*), conditional splash regime (*II*), and no splash regime (*III*). In the splash regime (*I*), an impact droplet splashed, regardless of the stretchability of the membrane; however, there was no splash in region (*III*). Region (*II*) is the boundary between regions (*I*) and (*III*); in this region, the occurrence of a splash depended on the stretchability. For example, the conditions shown in Figure 4a (with *We* = 53) correspond to region (*II*). The *We* of both droplets impinging on the stretchable (ε = 100%) and rigid surfaces are the same, but the occurrence of splashing is totally different. The morphology of the droplets, as well as the splashing, depended on the state of the surface. For instance, the droplet in region (*III*) became elongated and ejected a satellite droplet onto the rigid membrane; however, on the stretchable membrane, the droplet spread in all directions and eventually merged before bouncing back (Supporting Information Figure S6a). Bouncing is one of the most unique properties of the superhydrophobic surface. In general, some of the initial kinetic energy dissipates after impact. The coefficient of restitution (COR) is a parameter that reveals the height of the bounce and how much kinetic energy is

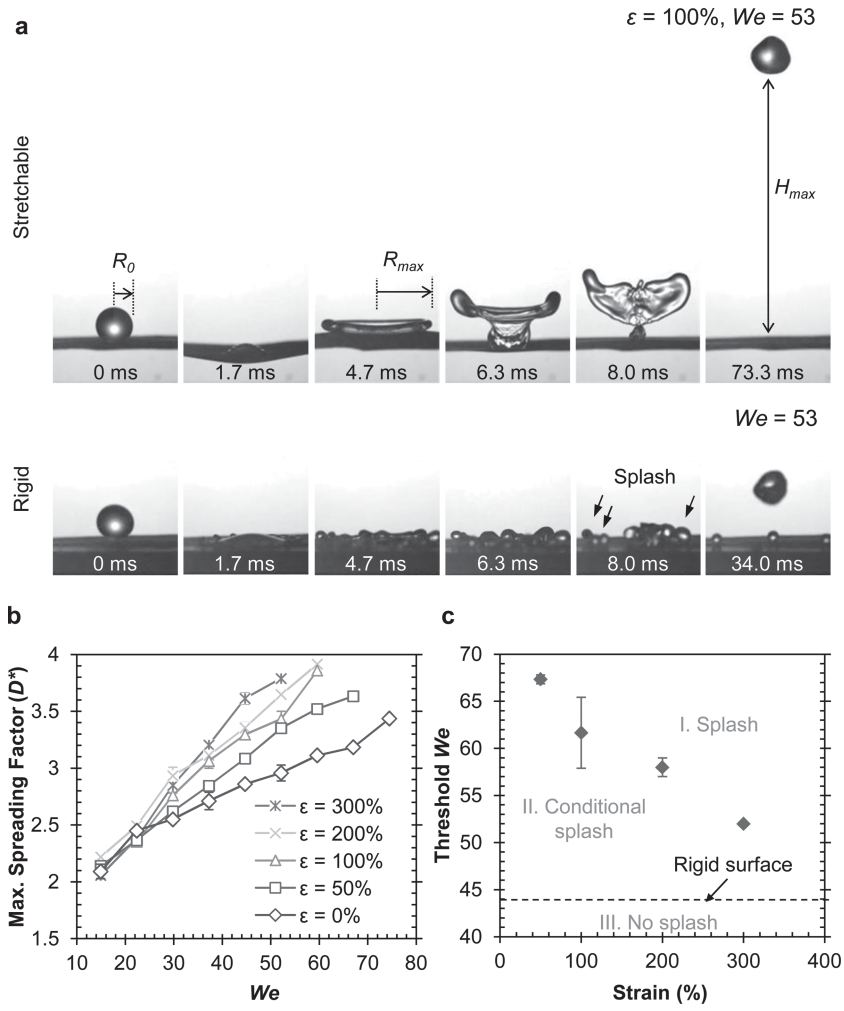

Figure 4. a) Sequential optical images of droplet impact on a stretchable (100% stretched) and a rigid superhydrophobic surface. (Impact velocity of the droplet: 1.67 m s^{-1}; Weber number, *We*: 53). The impinging droplet exhibited different behavior for the different surfaces. Under the same *We*, the droplet splashed just after spreading on the rigid superhydrophobic surface, which was supported by an aluminum block beneath the stretchable membrane; however, on the stretchable surface, the droplet spread in all directions but eventually merged as it bounced back. b) Maximum spreading factor, $D^* = R_{max}/R_0$, with different *We* of various strains. c) Threshold *We* for splashing vs. strain. This Figure is divided into the splash regime (*I*), conditional splash regime (*II*), and no splash regime (*III*). In the splash regime (*I*), an impact droplet splashed, regardless of the stretchability of the membrane; however, there was no splash in region (*III*). Region (*II*) is the boundary between regions (*I*) and (*III*); in this region, the occurrence of a splash depended on the stretchability. Above the threshold *We*, the droplet splashed as shown in the bottom sequential images of (a); but below the threshold, there was no splash. The dashed line at 44 is the splash threshold on a rigid surface, and it is lower than any other stretchable surface. More analysis and movies about the droplet impact can be found in the Supporting Information.

dissipated. The COR is defined as $\sqrt{H_{max}/H_0}$ where H_0 and H_{max} are the initial height and maximum bounce height, respectively. According to optical analysis, the rigid membrane has a high COR (0.28), compared with the elastic membrane (0.21–0.27), and the COR tended to decrease as the strain increased (Supporting Information Figure S7). In summary, the stretchable, superhydrophobic membrane tended to suppress splashing, ejection, and bouncing, compared with the rigid superhydrophobic surface.

2.4. Evaluation of the Gas Breathability and Underwater Gas Sensing

The micropores in the fibrous membrane provide excellent gas breathability. To evaluate the breathability, we set up a gas chamber connected to an O_2 gas source, as shown in **Figure 5**a. The chamber was divided by our gas-breathable membrane, and the O_2 concentration in each space was measured by an O_2 gas sensor, with the concentration controlled by a valve. Figure 5b plots the O_2 concentration that passed through the membrane (Sensor 2) *versus* the reference O_2 concentration in the supplied gas (Sensor 1). The O_2 concentrations in the two spaces show excellent linearity over the entire concentration range. This implies that the membrane has superior gas breathability. Additionally, to compare breathability at various strains, the O_2 concentrations measured with Sensors 1 and 2 were compared after blowing O_2-mixed air (O_2 concentration of 24–26%) into the chamber. In the stretched condition, the breathability was maintained regardless of the strain, as shown in Figure 5c. The diffusion in the porous membrane was due mainly to molecular collisions because the pores (>5 μm) were much larger than the molecular mean free path of the diffusing gas (in this case, the mean free path of oxygen at atmospheric pressure and room temperature was approximately 100 nm). The scale of the pores did not change significantly when the membrane was stretched. Therefore, the pores allowed efficient gas diffusion through the membrane regardless of the membrane strain.

A stretchable, gas-breathable superhydrophobic membrane would have many applications. Here, we demonstrated a novel functional membrane packaging for an underwater gas sensor as one application. Generally, a gas sensor operates in a gaseous environment. Therefore, it is difficult to measure gas under water, as in bubbles. Figure 5d shows an O_2 gas sensor packaged in our membrane. The membrane adhered tightly to the gas sensor thanks to its stretchability. When the sensor was immersed in water, the membrane appeared silver because of the total reflection of air trapped on the superhydrophobic surface (Cassie state), as seen in Figure 5e (the inset image is the membrane in air). The superhydrophobic surface had a high contact angle and a very low contact angle for a bubble, almost 0°, so that a bubble in water was readily absorbed on the membrane (Figure 5f). Figure 5g shows the detection of O_2 bubbles underwater using the packaged gas sensor. The O_2 concentration increased with the number of bubbles captured. Furthermore, because of the

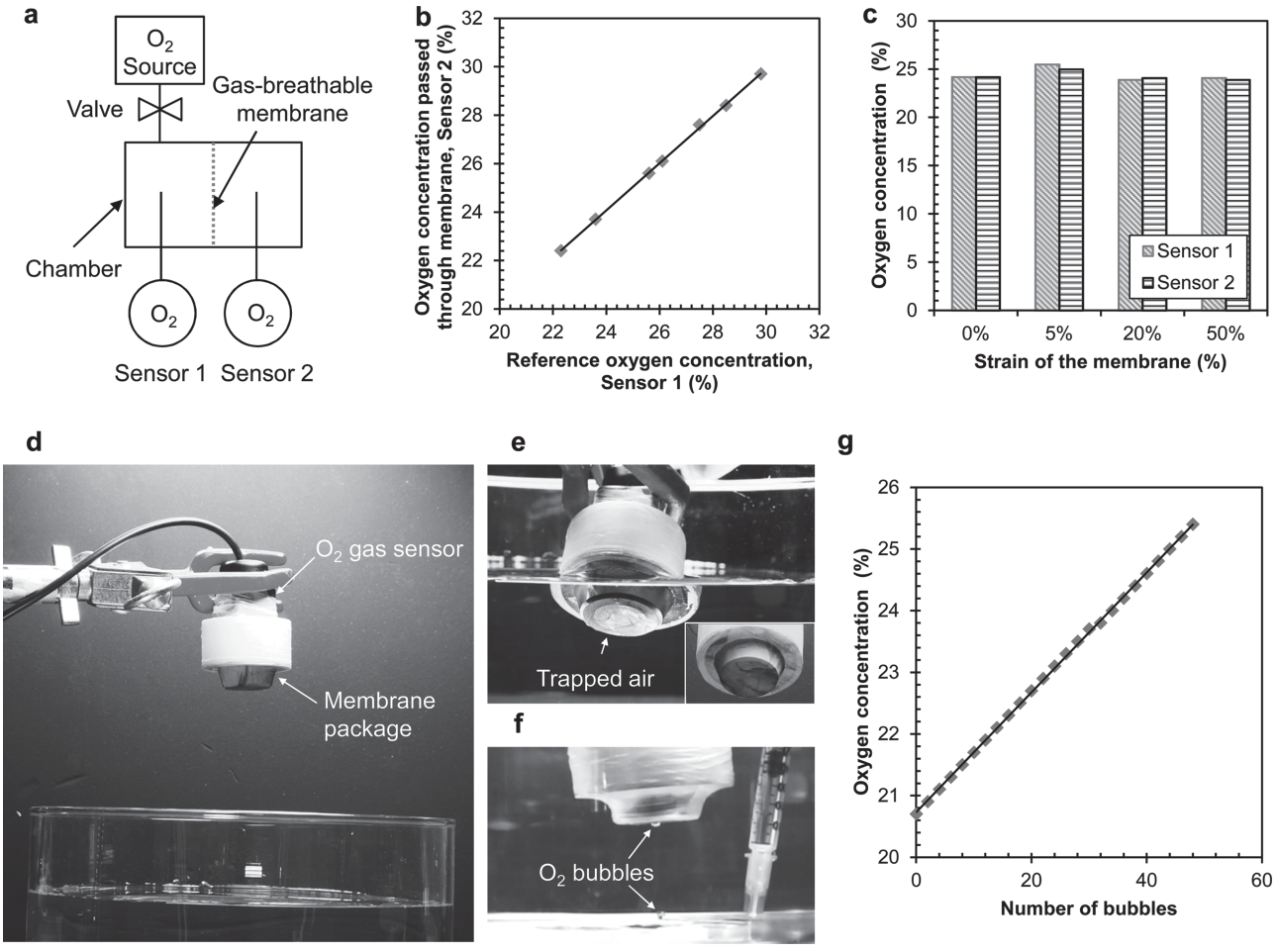

Figure 5. a) Schematic of the set-up used to evaluate air breathability. b) A plot of the O_2 concentration that passed through the membrane (Sensor 2) versus the reference O_2 concentration in the supplied gas (Sensor 1). c) O_2 concentrations at various strains. The concentration in the membrane was remarkably consistent with the reference concentration. d) Image of the functional membrane packaging for an underwater gas sensor. e) Packaged sensor in water. The shiny surface is due to the trapped air on the superhydrophobic membrane. The inset shows the same membrane in (f). The moment when the O_2 bubble in water was absorbed into the membrane. g) Detection of O_2 bubbles underwater using the packaged gas sensor.

excellent waterproofing arising from the superhydrophobicity of the membrane, the gas sensor and electric circuit were never exposed to water during the underwater testing.

3. Conclusions

We have successfully developed a novel, superhydrophobic nanostructured fibrous membrane with a rubberlike stretchability and gas breathability. This membrane was fabricated using simple, economical processes, including electrospinning and dilute polymerization. The membrane maintained excellent superhydrophobicity under harsh dynamic conditions, such as cyclical stretching. The membrane's high durability and superhydrophobicity were attributed to regularly formed cracks in the fibers of the nanostructures. These cracks in the fibers helped to release the interfacial stress that occurred during the high deformation and minimized the contact area between the liquid–solid interface, due to the hierarchical architecture consisting of microfibers, nanostructures on fibers, and ordered cracks. We also observed that the stretchable membrane exhibited unique impact behaviors, such as the suppression of splashing, ejecting, and bouncing, compared with the typical hard superhydrophobic surface. However, the impact behaviors on stretchable superhydrophobic surfaces are not fully understood; thus, further study is needed. Lastly, we evaluated the gas breathability and demonstrated underwater gas sensing as a novel application. Our unique membrane will provide new insight into dynamic droplet manipulation and the development of functional clothes, packaging of stretchable electronics, and gas–liquid exchange applications.

4. Experimental Section

Electrospun Polyurethane Fibrous Membrane: A thermoplastic polyurethane elastomer (PU) (Pellethane 2363-80AE, Lubrizol, USA) was used as received, without further purification. The PU was dissolved in a 13 wt% mixture of tetrahydrofuran (THF) and dimethylformamide (DMF) (60/40, v/v). Electrospinning was conducted at room temperature and low humidity (relative humidity of 30–40%). The electrospinning setup

and procedure were the same as those used in our previous work.[29] After electrospinning, the membranes were affixed to a plastic holder to maintain their shape during the post-process. Aligned fibers were produced with a trenched collector.[28,29]

Surface Modification: Polyaniline (PANI) nanofibrous structures were synthesized on the electrospun PU membrane using dilute chemical polymerization.[23] The PU membrane was immersed in an aqueous solution containing 1 M $HClO_4$ (Samchun Pure Chemical, Korea), 6.7 mM ammonium persulfate (APS, Sigma Aldrich, USA), and 10 mM aniline monomer (Sigma Aldrich, USA). The aniline monomers were polymerized at a temperature of 0–4 °C, with 12 h of agitation (shaking of the mixture). After synthesis, the membranes were rinsed in a deionized (DI) water flow to remove the remaining PANI residue. The membranes were then dried using N_2 gas and placed in a desiccator for 1 day. Finally, the prepared membranes were dip-coated in a 2% PTFE solution (Teflon AF 601S1-100-6, Dupont, USA) which was diluted in FC-75 (Acros Organics, Belgium) and cured on a 65 °C hotplate for 10 min.

Measurements for Characteristics: Contact angle (CA) and contact angle hysteresis (CAH) were measured according to the trajectory of 5-μL DI water droplets with respect to the nanostructured surface, using a droplet-shape analysis system (DSA 100, Kruss, Germany) and the sessile droplet method. CAH was calculated from the difference between the advancing contact angle and the receding contact angle. The velocity of the 10-μL droplets in the impact experiment was controlled by varying the height of the pipette (0.5–10 μL, BioHIT, Finland). The impacts were recorded using a high-speed camera (Fastcam SA3, Photron, USA) at 3000 frames per second and 1/20000 s shutter speed, with backlighting for improved contrast. The diameter of the droplet and height were analyzed optically. The horizontality of the membrane was calibrated using an X–Y tiling stage. For evaluation of gas breathability, a phenolphthalein pH indicator solution and an ammonia solution (a volatile base) were used. Phenolphthalein (Sigma Aldrich) was dispersed in a 1 wt% mixture of DI water/methanol (90/10, v/v). The ammonia solution (30% in water, Samchun Chemical, Korea) was used without further processing. The stress–strain curves of the electrospun PTFE-PU fibers and PTFE-PANI-coated fibers were obtained with a universal testing system (Nano Bionix, MTS Nano Instruments) at a crosshead speed of 27 μm s^{-1} at room temperature. The O_2 concentration was monitored with a digital oxygen indicator (XO-326ALA; New Cosmos Electric, Japan) and DO-5Z (KRK, Japan).

Supporting Information

Supporting Information is available from the Wiley Online Library or from the author.

Acknowledgements

This work was supported by the National Research Foundation of Korea (NRF) grant funded by the Korea government (MEST) (No. 2012R1A2A2A06047424).

Received: February 3, 2013
Revised: March 28, 2013
Published online: June 6, 2013

[1] R. Blossey, *Nat. Mater.* **2003**, *2*, 301–306.
[2] L. Cao, A. K. Jones, V. K. Sikka, J. Wu, D. Gao, *Langmuir* **2009**, *25*, 12444–12448.
[3] C.-H. Choi, C.-J. Kim, *Phys. Rev. Lett.* **2006**, *96*, 066001–4.
[4] A. R. Parker, C. R. Lawrence, *Nature* **2001**, *414*, 33–34.
[5] L. Feng, Z. Zhang, Z. Mai, Y. Ma, B. Liu, L. Jiang, D. Zhu, *Angew. Chem. Int. Ed.* **2004**, *43*, 2012–2014.
[6] H. S. Lim, J. H. Baek, K. Park, H. S. Shin, J. Kim, J. H. Cho, *Adv. Mater.* **2010**, *22*, 2138–2141.
[7] Z. Guo, F. Zhou, J. Hao, W. Liu, *J. Am. Chem. Soc.* **2005**, *127*, 15670–15671.
[8] T. An, S. J. Cho, W. Choi, J. H. Kim, S. T. Lim, G. Lim, *Soft Matter* **2011**, *7*, 9867–9870.
[9] A. Tuteja, W. Choi, M. Ma, J. S. Mabry, S. A. Mazzella, G. C. Rutledge, G. H. McKinley, R. E. Cohen, *Science* **2007**, *318*, 1618–1622.
[10] X. Deng, L. Mammen, H.-J. Butt, D. Vollmer, *Science* **2012**, *335*, 67–70.
[11] M. Xu, N. Lu, H. Xu, D. Qi, Y. Wang, S. Shi, L. Chi, *Soft Matter* **2010**, *6*, 1438.
[12] T. Yao, C. Wang, Q. Lin, X. Li, X. Chen, J. Wu, J. Zhang, K. Yu, B. Yang, *Nanotechnology* **2009**, *20*, 065304.
[13] S. E. Lee, D. Lee, P. Lee, S. H. Ko, S. S. Lee, S. U. Hong, *Macromol. Mater. Eng.* **2013**, DOI:10.1002/mame.201200098.
[14] S. Lee, J. H. Kang, S. J. Lee, W. Hwang, *Lab. Chip* **2009**, *9*, 2234.
[15] T. M. Schutzius, M. K. Tiwari, I. S. Bayer, C. M. Megaridis, *Composites, Part A* **2011**, *42*, 979–985.
[16] J. Zhang, X. Lu, W. Huang, Y. Han, *Macromol. Rapid Commun.* **2005**, *26*, 477–480.
[17] J. Zhang, J. Li, Y. Han, *Macromol. Rapid Commun.* **2004**, *25*, 1105–1108.
[18] D. Wu, S. Wu, Q. Chen, Y. Zhang, J. Yao, X. Yao, L. Niu, J. Wang, L. Jiang, H. Sun, *Adv. Mater.* **2011**, *23*, 545–549.
[19] J. Catanese III, D. Cooke, C. Maas, L. Pruitt, *J. Biomed. Mater. Res.* **1999**, *48*, 187–192.
[20] A. L. Yarin, *Annu. Rev. Fluid Mech.* **2006**, *38*, 159–192.
[21] A. Greiner, J. H. Wendorff, *Angew. Chem. Int. Ed.* **2007**, *46*, 5670–5703.
[22] W. Barthlott, C. Neinhuis, *Planta* **1997**, *202*, 1–8.
[23] N.-R. Chiou, C. Lu, J. Guan, L. J. Lee, A. J. Epstein, *Nat. Nanotechnol.* **2007**, *2*, 354–357.
[24] K. Lee, B. Lee, C. Kim, H. Kim, K. Kim, C. Nah, *Macromol. Res.* **2005**, *13*, 441–445.
[25] H. Valentová, J. Stejskal, *Synth. Met.* **2010**, *160*, 832–834.
[26] D. H. Reneker, A. L. Yarin, H. Fong, S. Koombhongse, *J. Appl. Phys.* **2000**, *87*, 4531.
[27] K. H. Nam, I. H. Park, S. H. Ko, *Nature* **2012**, *485*, 221–224.
[28] B. Kim, S. J. Cho, T. An, H. Ryu, H. Lim, G. Lim, *Phys. Status Solidi RRL* **2012**, *6*, 409–411.
[29] S. J. Cho, B. Kim, T. An, G. Lim, *Langmuir* **2010**, *26*, 14395–14399.
[30] G. B. Foote, P. S. Du Toit, *J. Appl. Meteor.* **1969**, *8*, 249–253.
[31] S. Wang, L. Jiang, *Adv. Mater.* **2007**, *19*, 3423–3424.
[32] C. Clanet, C. BéGuin, D. Richard, D. QuéRé, *J. Fluid Mech.* **2004**, *517*, 199–208.
[33] H. Kim, C. Lee, M. H. Kim, J. Kim, *Langmuir* **2012**, *28*, 11250–7.
[34] R. E. Pepper, L. Courbin, H. A. Stone, *Phys. Fluids* **2008**, *20*, 082103–8.